JACS
JOURNAL OF THE AMERICAN CHEMICAL SOCIETY
Article
Cite This: J. Am. Chem. Soc. XXXX, XXX, XXX−XXX
pubs.acs.org/JACS

Ultrabright and Fluorogenic Probes for Multicolor Imaging and Tracking of Lipid Droplets in Cells and Tissues

Mayeul Collot,*[,†] Tkhe Kyong Fam,[†] Pichandi Ashokkumar,[†] Orestis Faklaris,[‡] Thierry Galli,[§,∥] Lydia Danglot,[§,∥] and Andrey S. Klymchenko[†]

[†]Laboratoire de Biophotonique et Pharmacologie, CNRS UMR 7213, Université de Strasbourg, Faculté de Pharmacie, 74, Route du Rhin, 67401 Illkirch, France

[‡]ImagoSeine Core Facility, Institut Jacques Monod, Université Paris Diderot/CNRS, UMR 7593, 15 Rue Hélène Brion, 75205 Paris CEDEX 13, France

[§]INSERM U894, Centre de Psychiatrie et Neurosciences, "Membrane Traffic in Health and Diseased Brain" Team, 102-108 Rue de la Santé, 75014 Paris, France

[∥]Université Paris Descartes, 75014 Paris, France

Supporting Information

ABSTRACT: Lipid droplets (LDs) are intracellular lipid-rich organelles that regulate the storage of neutral lipids and were recently found to be involved in many physiological processes, metabolic disorders, and diseases including obesity, diabetes, and cancers. Herein we present a family of new fluorogenic merocyanine fluorophores based on an indolenine moiety and a dioxaborine barbiturate derivative. These so-called StatoMerocyanines (SMCy) fluoresce from yellow to the near-infrared (NIR) in oil with an impressive fluorescence enhancement compared to aqueous media. Additionally, SMCy display remarkably high molar extinction coefficients (up to 390 000 M^{-1} cm^{-1}) and high quantum yield values (up to 100%). All the members of this new family specifically stain the LDs in live cells with very low background noise. Unlike Nile Red, a well-known lipid droplet marker, SMCy dyes possess narrow absorption and emission bands in the visible, thus allowing multicolor imaging. SMCy proved to be compatible with fixation and led to high-quality 3D images of lipid droplets in cells and tissues. Their high brightness allowed efficient tissue imaging of adipocytes and circulating LDs. Moreover their remarkably high two-photon absorption cross-section, especially SMCy5.5 (up to 13 300 GM), as well as their capacity to efficiently fluoresce in the NIR region led to two-photon multicolor tissue imaging (liver). Taking advantage of the available color palette, lipid droplet exchange between cells was tracked and imaged, thus demonstrating intercellular communication.

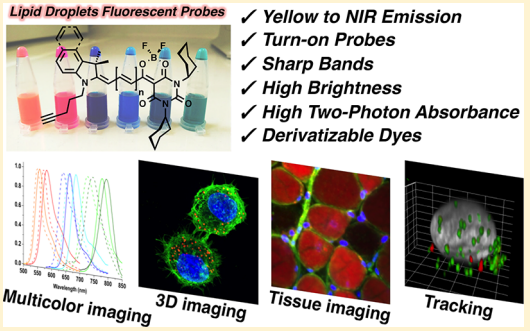

INTRODUCTION

Lipid droplets (LDs), also known as adiposomes or lipid bodies, are intracellular lipid-rich organelles that regulate the storage of neutral lipids including triglycerides and cholesterol esters.[1,2] Although LDs are mainly found in adipose tissue, nearly all cells are capable of storing lipids in these reservoirs, as this ability to store such a source of metabolic energy is crucial for survival.[3,4] It has been shown that cells other than adipocytes can form LDs as a response to a stress.[4] In recent years, LDs have drawn considerable attention, as they were found to be involved in many physiological processes including membrane synthesis and trafficking,[5,6] protein degradation,[7] but also inflammation[8] and pathologies including obesity, diabetes, and atherosclerosis[9] as well as viral replication[10] and cancer.[11−13] Therefore, imaging and tracking LDs is of prior importance. The rise of fluorescence imaging techniques stimulated the development of efficient molecular fluorescent probes specific for various physiological phenomena or able to specifically stain organelles including mitochondria, the nucleus, and the plasma membrane.[14−17] In particular, one should mention fluorogenic probes that turn on their emission only after binding to the biological target, allowing background-free bioimaging.[18−21] However, examples of probes for LDs are still limited. Nile Red is a commercially available solvatochromic dye (Figure 1A) that was reported to stain LDs[22] and is the most commonly used LD marker. However, Nile Red suffers from several drawbacks: (i) nonspecific staining of other organelles (particularly lipid membranes) and (ii) broad absorption and emission spectra that limit the possibilities for multicolor imaging. Although recent efforts have been made to develop new LD probes based on various fluorophores including BODIPY (496/503,[23] 540[24]), AIEgens (aggregation induced emission fluorophores),[25] azafluorenone,[26] and benzothiadiazole,[27] only one example of a far-red-emitting LD marker was recently published.[28] However, the latter, based

Received: December 21, 2017
Published: February 15, 2018

DOI: 10.1021/jacs.7b12817
J. Am. Chem. Soc. XXXX, XXX, XXX−XXX

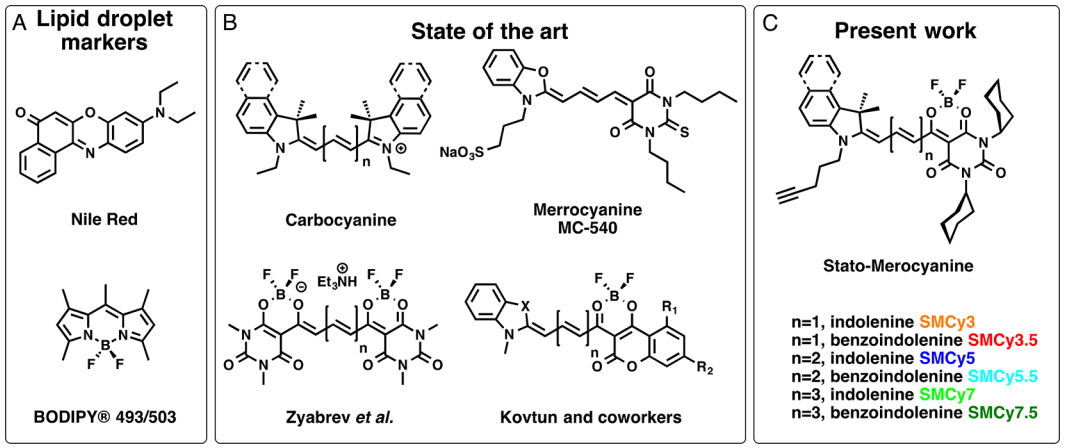

Figure 1. (A) Commonly used LD probes. (B) Structure of various cyanines including the pioneer work on dioxaborine cyanines. (C) The six members of the StatoMerocyanines family.

on AIEgen, suffers from a broad emission spectrum emitting in both the far-red and near-infrared (NIR) regions and was used at high concentrations (10 μM) probably due to its low quantum yield (0.05). In addition to emitting at the far-red and NIR wavelengths, the probe should be excitable at an optical window suitable for optimal tissue penetration (670−910 nm), which can be achieved from the two-photon excitable fluorescent probes with high two-photon-absorption (TPA) cross-section.[29] Therefore, bright and selective LD probes, compatible in multicolor imaging and operating in the far-red and NIR region, are in demand. Cyanines are one of the most famous and widely used fluorophores. Their emission color spans from the visible range to the NIR and constitute a platform for biomolecule labeling[30] and for the development of chemosensors for bioimaging.[31,32] Among cyanines one can differentiate the cationic carbocyanines and the noncharged merocyanines (Figure 1B). Carbocyanines are bright fluorophores, but their positive charge can be detrimental for designing specific fluorescent probes, as it has a tendency to provoke attraction toward negatively charged biomolecules (proteins and biomembranes) by opposite charge attractions. Merocyanines circumvent this problem, as the core fluorophore generally does not display any charges. Unfortunately, in many cases merocyanines are nonphotostable. Conversely, BODIPY are generally neutral, bright, and stable fluorophores due to their planar structures stabilized by a difluoroboron complex that reduces the rotations and vibrations. Consequently, fluorophores including merocyanines stabilized with a rigid boron bridge (dioxaborine complex) are drawing continuous attention in the field of bioimaging. Indeed these fluorophores served in cellular imaging either in molecular form[33−35] or incorporated in nanoparticles,[36−38] as well as for imaging the nucleus,[39] sensing oxygen[40,41] or DNA,[42,43] and imaging ligand receptor interactions.[44]

Barbiturate-based merocyanines have been known for decades. MC-540 (Figure 1B), a fluorescent probe for lipid membranes,[45] is a figurehead of this family. Although it is a bright red emitting fluorophore, it suffers from a low photostability and high phototoxicity. The dioxaborine barbituryl moiety was first introduced by Zyabrev et al. and served to develop bright negatively charged dyes (Figure 1B).[46] In parallel, fluorophores incorporating dioxaborine complexes and indolenine moieties were intensively studied by Kovtun and co-workers (Figure 1B).[47−49]

Herein, we developed a family of new merocyanine fluorophores based on an indolenine moiety and a dioxaborine barbiturate derivative separated by a polymethyne chain of various lengths (Figure 1). These so-called StatoMerocyanines (SMCy) have a fluorescence spanning from yellow to the NIR and display a bright fluorescence due to high molar extinction coefficients and high quantum yield values. SMCy are fluorogenic, as they are nonemissive in aqueous media and stain the lipid droplets of cells in a bright and selective manner. Additionally, due to their narrow absorption and emission bands, SMCy showed their efficiency in multicolor imaging compared to Nile Red and successfully served for multicolor tissue imaging. SMCy dyes were shown to possess remarkably high two-photon absorption cross-sections (up to more than 10 000 GM) and were successfully used in multicolor two-photon excitation (TPE) tissue imaging. Finally we used SMCy probes to track two populations of LDs, and we demonstrated that LD exchange occurs between cells.

RESULTS AND DISCUSSION

Synthesis. Herein we introduce the SMCy fluorophores that arose from the stabilization of a barbiturate-based merocyanine by a dioxaborine bridge that fixes (*stativus* in latin) a degree of rotation of the fluorophore and therefore enhances its brightness (Figure 1C).

SMCy dyes are composed of (1) an indolenine moiety bearing a pentynyl tail that reinforces the hydrophobicity and allows the opportunity to functionalize the dye by copper(I)-catalyzed alkyne−azide cycloaddition (CuAAC), if needed, and (2) a dioxaborine barbituric moiety bearing two cyclohexyl rings that were chosen for their hydrophobicity and bulkiness that can help in preventing formation of nonemissive H-aggregates by π-stacking.[50−52]

The synthesis involved the acetylation of dicyclohexylbarbituric acid **1** in the presence of $BF_3{\cdot}OEt_2$ to form the dioxaborine barbituryl **2** (Scheme 1). The latter was then condensed on hemicyanines with various polymethine chain lengths in pyridine to provide the SMCy dyes.

The same nomenclature as the one introduced by Ernst et al. for the carbocyanines[53] was used. The suffix number indicates the number of carbons separating the indole ring from the dioxaborine barbituryl and the ".5" depicts the use of the extended benzoindolenine moiety instead of indolenine (Figure 1C). The obtained fluorophores were characterized by ^{1}H, ^{13}C,

DOI: 10.1021/jacs.7b12817
J. Am. Chem. Soc. XXXX, XXX, XXX−XXX

Scheme 1. Synthesis of SMCy Dyes

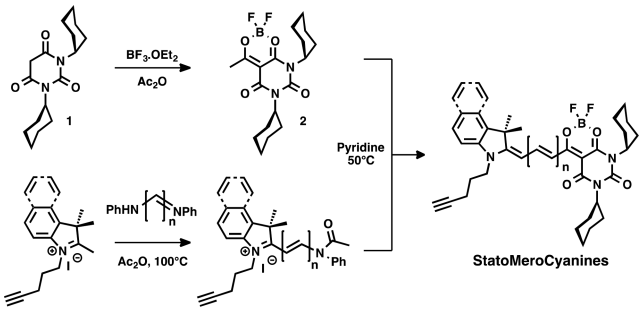

and ^{19}F NMR as well as high-resolution mass spectrometry. Additionally, the structure of SMCy7 was confirmed by X-ray diffraction and showed a planar structure with minimal twist of the polymethine chain as well as the bulkiness induced by the cyclohexyl moieties (Figure 2).

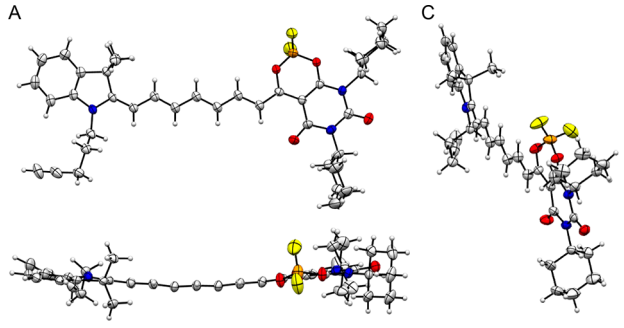

Figure 2. ORTEP representation of SMCy7 obtained by X-ray diffraction of a single crystal. (A) Side view, (B) top view, and (C) diagonal view. For clarity, heteroatoms were colored: Boron (orange), nitrogen (blue), oxygen (red), and fluorine (yellow).

Spectroscopic Studies. The photophysical properties of SMCy dyes were first studied in 10 various organic solvents with increasing polarity from toluene to DMSO and are summarized in Table 1 (all spectra are available in the Supporting Information). First, the SMCy mostly displayed narrow absorption and emission spectra and their absorption wavelengths span from 526 to 770 nm and their emission wavelengths from 550 to 794 nm (Figure 3). The use of the benzoindolenine instead of the indolenine moiety, giving rise to the ".5" markers, typically provoked a ~20 nm bathochromic

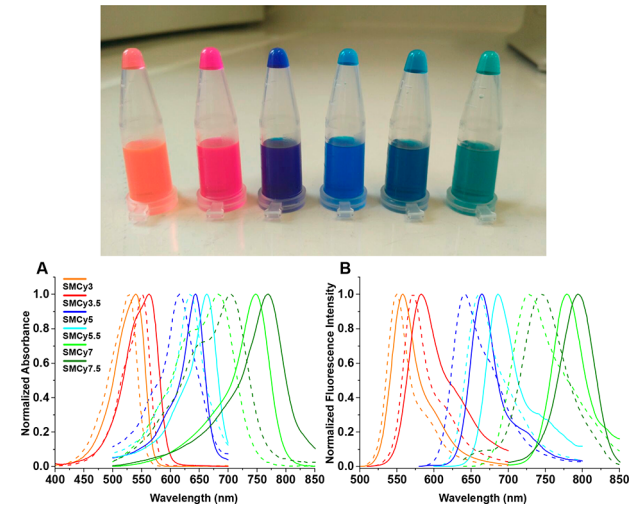

Figure 3. Top: Picture of the SMCy in solution (200 μM in DMSO). From left to right: SMCy3, SMCy3.5, SMCy5, SMCy5.5, SMCy7, and SMCy7.5. Bottom: Normalized absorption spectra (A) and normalized emission spectra (B) of SMCy3 to SMCy7.5 in toluene (dashed lines) and in DMSO (solid lines). Concentrations were 1 μM for SMCy3, SMCy3.5, SMCy7, and SMCy7.5 and 200 nM for SMCy5 and SMCy5.5. Excitations were 490 nm for SMCy3 and SMCy3.5, 560 nm for SMCy5, 590 nm for SMCy5.5, 630 nm for SMCy7, and 630 and 690 nm for SMCy7.5.

shift in both absorption and emission spectra. All SMCy exhibited positive solvatochromism, as their absorption and emission spectra were significantly red-shifted in polar solvents. Moreover, the solvatochromic effect, as well as the Stokes shift, increases with the length of the polymethine chain. Indeed, whereas SMCy3 displayed only a 8 nm bathochromic emission shift from toluene to DMSO, SMCy7 displayed a 52 nm shift (Table 1). Weak solvatochromism for the dyes with shorter conjugation (SMCy3 and SMCy3.5) can be explained by their merocyanine type of electronic distribution, where the electronic charge of indolenine nitrogen is transferred to the barbiturate unit in the ground state without further strong change in the excited state. However, for dyes exhibiting longer conjugation this ground-state charge transfer is probably less pronounced, so that they undergo charge transfer in the excited state. The latter increases the dipole moment on electronic excitation, leading to significant solvatochromism in absorption and fluorescence, in line with the earlier report on other

Table 1. Photophysical Properties of SMCy Dyes in Toluene and DMSO[a]

probe	solvent	λ_{Abs} (nm)	ε (M^{-1} cm^{1})	$fwhm_{Abs}$ (nm)	λ Em (nm)	$fwhm_{Em}$ (nm)	Stokes shift	QY (ϕ)	brightness ($\varepsilon \times \phi$)
SMCy3	toluene	528	94 000	52	550	33	22	0.3	28 200
	DMSO	540	77 300	57	558	40	18	0.37	28 600
SMCy3.5	toluene	551	124 000	51	572	37	21	0.68	84 320
	DMSO	563	110 000	64	583	56	20	0.18	19 800
SMCy5	toluene	615	203 000	61	642	63	27	0.35	71 000
	DMSO	644	363 000	42	665	39	21	0.42	152 400
SMCy5.5	toluene	634	168 000	52	661	53	27	0.65	109 200
	DMSO	663	241 200	50	687	44	24	0.26	62 700
SMCy7	toluene	683	109 000	114	727	84	44	0.21	22 890
	DMSO	748	231 000	67	779	49	31	0.33	76 230
SMCy7.5	toluene	705	89 000	116	746	67	41	0.18	16 020
	DMSO	770	183 000	78	794	53	24	0.18	32 900

[a] ε is the molar extinction coefficient, fwhm is the full width at half-maximum, and the Stokes shifts are expressed in nm.

DOI: 10.1021/jacs.7b12817
J. Am. Chem. Soc. XXXX, XXX, XXX−XXX

asymmetrical cyanine dyes.[54] SMCy3 and SMCy3.5 also slightly differ from the other SMCy. First, whereas hypochromism was observed with increasing solvent polarity, the other SMCy displayed hyperchromism (Figures and Tables S1 to S6). Then, whereas other SMCy have shortened full widths at half-maximum (fwhm) with increasing solvent polarity, SMCy3 and SMCy3.5 did not display significant changes in their spectra. In addition, the brightness of SMCy is highly dependent on the nature of the solvent; they generally display high molar extinction coefficients ranging from 77 000 to an impressive value of 394 000 M^{-1} cm^{-1}, and their quantum yield values vary from 0.07 to 0.76 (see SI). Among the SMCy dyes, SMCy5 was found to be the brightest, with a maximum brightness of 227 500 M^{-1} cm^{-1} in dichloromethane (DCM), competing with the squaraine dyes[55] and thus constituting one of the brightest small molecules to date.[56,57] As mentioned earlier, the photostability of merocyanine can be a limitation for their use in bioimaging; therefore the photostability of SMCy dyes was evaluated. SMCy3 and SMCy5 were continuously irradiated in a cuvette for 1 h in dioxane. Their photostability was monitored and compared to fluorophores with similar spectral properties: MC-540, a barbiturate-based merocyanine, and DID, a far-red-emitting carbocyanine 5,[23] respectively. The results showed that both SMCy3 and SMCy5 displayed higher photostability compared to the merocyanine and the carbocyanine (Figure S7).

In the light of the high lipophilic nature of the SMCy dyes, their photophysical properties were measured in oils—colza oil (mainly composed of unsaturated long chain triglycerides) and in Labrafac (a medium chain triglyceride containing oil)—as well as in water. The results showed first that, despite their high lipophilic nature, SMCy can be suspended in water: their significantly broadened absorption spectra suggest that they actually form soluble aggregates (Figure 4A and Figures S12 and S13). Consequently, SMCy are nonemissive in water (Figure 4B). In oils, SMCy dyes display high brightness similar to or higher than those obtained in nonpolar solvents, thus providing impressive fluorescence enhancements (up to 1700-fold) compared to water (Table 2). It is also noteworthy that, in these lipophilic environments, all the SMCy dyes are efficiently excited with the commonly available lasers (488, 560, and 630 nm). Remarkably, SMCy5 and SMCy5.5 exhibit the highest brightness, especially in Labrafac, reaching high quantum yields of 0.74 and 1.00, respectively. Higher quantum yields of SMCy in oils compared to organic solvents could be linked to additional restriction of intramolecular rotation in viscous media, in line with a previous report on a push−pull dioxaborine derivative.[44] The photostability in oil of SMCy3 and SMCy5 was compared to commercially available LD markers, namely, BODIPY 493/503 and Nile Red. Whereas BODIPY 493/503 and SMCy5 lost 15% fluorescence intensity after 1 h of irradiation in the cuvette, SMCy3 displayed high photostability similar to Nile Red (Figure S8). According to the present results, SMCy appeared as suitable candidates to probe neutral lipophilic environments such as LDs in cells, using fluorescence microscopy techniques.

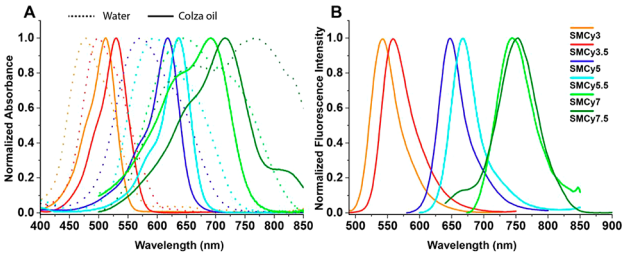

Figure 4. Normalized absorption spectra of SMCy dyes (1 μM) in water (dashed lines) and in colza oil (solid lines) (A) and their normalized emission spectra in oil (B). Excitation wavelength was 480 nm for SMCy3 and SMCy3.5, 560 nm for SMCy5, 590 nm for SMCy5.5, and 630 nm for SMCy7 and SMCy7.5.

CELLULAR EXPERIMENTS

Localization of SMCy. On the basis of their chemical properties described above, SMCy were incubated with KB cells (HeLa cells derivatives), and the fluorescence was monitored over the time. After several minutes of incubation in a starvation medium (Hank's balanced salt solution, HBSS), a selective and intense fluorescence was observed in vesicles slowly moving in the cytoplasm of the cells (see Movie 1). The slow motion of these vesicles as well as their size and spherical shape led us to think that it was LDs. In order to confirm our expectations, a colocalization experiment was performed using Nile Red as a reference LD marker. As mentioned, Nile Red is a solvatochromic fluorophore with broad emission spectra and therefore can hardly be used for colocalization experiments with green- and red-emitting fluorophores due to crosstalk between the imaging channels. Thus, after checking that crosstalk did not occur in the NIR channel (excitation at 635 nm) (Figure S9), SMCy7 that emits in the NIR (730 nm) was first colocalized with Nile Red (Figure 5A). The results confirmed a clear colocalization between Nile Red and SMCy7. Consequently SMCy7 was used in combination with SMCy3 and SMCy3.5 (Figure 5B and C), and SMCy3 was then used to colocalize with SMCy5 and SMCy5.5 (Figure 5D and E). These experiments confirmed that the SMCy dyes selectively mark the LDs. In order to investigate the mechanism of staining, images have been taken at various times of incubation on live and fixed cells. The results showed a fluorescence enhancement in the LDs over time in both cells (see Figure S10). Consequently, we assume that SMCy accumulate in the LDs in a passive manner. The SMCy were also compared to BODIPY 493/503. Although SMCy dyes require incubation at 37 °C, BODIPY 493/503 immediately stained the LDs after addition (Figure S11). After investigating, we discovered that BODIPY 493/503 did not aggregate in water at concentrations as high as 1 μM with a quantum yield of 1.0. In sharp contrast, the turn-on SMCy LD sensors are nonfluorescent in water due to aggregation in the form of soluble nanoparticles even at 100 nM concentration (Figures S12 and S13). Additionally, BODIPY 493/503 was shown to be less selective (Figures S14 and S15) and less photostable than SMCy3 (Figure S16). At this stage of our work, cytotoxicity studies (MTT assay) were performed, and the results showed that at concentrations up to 5 μM the SMCy did not lead to any significant cytotoxicity (Figure S17).

3D Imaging. 3D imaging with confocal microscopy is normally obtained by reconstruction of Z-stack images, and therefore it involves multiple laser scans of the sample leading to the photobleaching of the fluorophores. Therefore, high brightness and photostability of the fluorescent markers are required to obtain good-quality 3D images. Here, SMCy allowed 3D imaging of the LDs, revealing their subcellular localization in KB cells (Figure 6). In these experiments a 21 μm Z-stack was performed using 70 slices with three averaged

DOI: 10.1021/jacs.7b12817
J. Am. Chem. Soc. XXXX, XXX, XXX−XXX

Table 2. Photophysical Properties of StatoMerocyanines in Triglyceride Oils[a]

	solvent	$\lambda_{Abs}/\lambda_{Em}$ (nm)	Stokes shift (nm)	ε (M^{-1} cm^{-1})	fwhm Abs/Em (nm)	QY (ϕ)	brightness ($\varepsilon \times \phi$)	$\Delta F/F_0$
SMCy3	colza oil	512/541	29	82 900	54/49	0.21	17 409	423
	Labrafac	511/542	31	87 300	55/51	0.25	21 825	515
SMCy3.5	colza oil	530/559	29	100 000	57/55	0.40	40 000	674
	Labrafac	529/557	28	108 000	57/58	0.54	58 320	827
SMCy5	colza oil	618/648	30	256 000	54/46	0.60	153 600	1088
	Labrafac	617/644	27	270 000	54/49	0.74	199 800	1700
SMCy5.5	colza oil	638/662	24	169 000	52/42	0.74	125 060	1535
	Labrafac	636/660	24	194 000	52/43	1.00	194 000	1535
SMCy7	colza oil	692/744	52	44 000	134/75	0.42	18 480	55
	Labrafac	687/735	48	44 000	137/84	0.44	19 360	79
SMCy7.5	colza oil	716/753	37	103 000	125/71	0.19	19 570	203
	Labrafac	712/743	31	83 000	132/74	0.2	16 600	145

[a]Concentration of the dyes was 1 μM. $\Delta F/F_0$ is the fluorescence enhancement between oil and water. F_0 is the maximum fluorescence intensity in water.

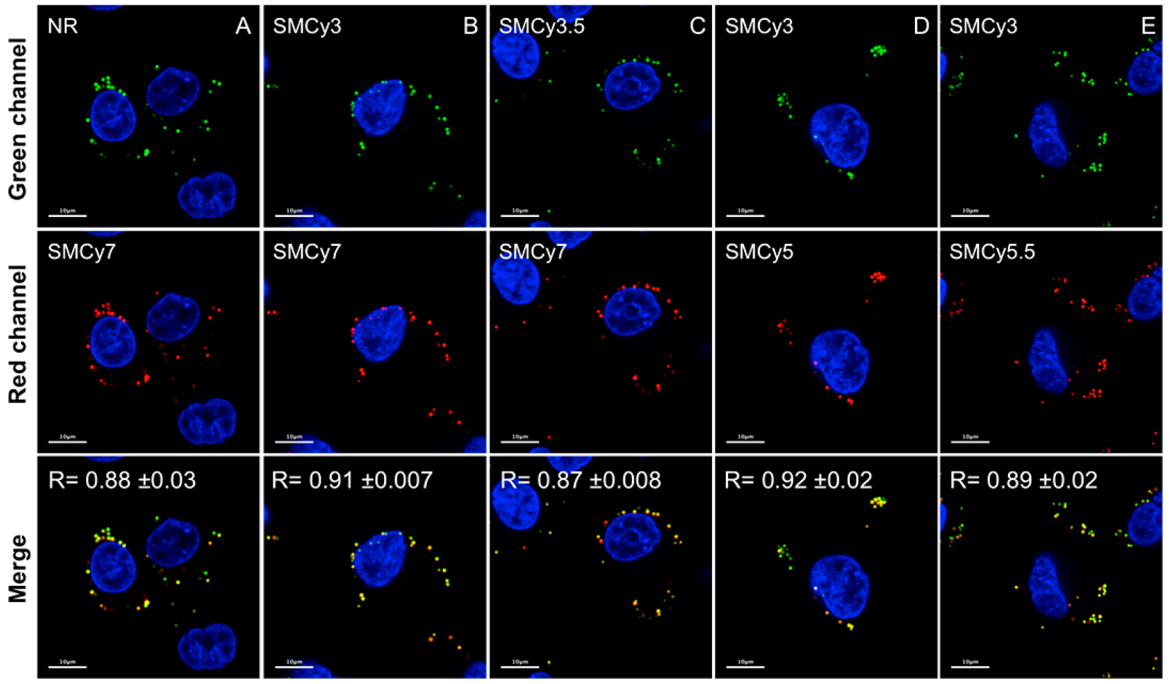

Figure 5. Laser scanning confocal microscopy of live KB cells incubated for 3 h in opti-MEM in the presence of fluorophores (500 nM). NR is Nile Red. Hoechst (5 μg/mL) was used to stain the nucleus (blue). Green channel: excitation at 488 nm, emission collected: 500−600 nm. Red channel (middle images): excitation at 635 nm, emission collected: 645−800 nm. The merged images correspond to the combined green and red channels. The displayed Pearson's correlation coefficient, which denotes the goodness of colocalization, is the average of at least five different images. Scale bar is 10 μm.

acquisitions per slice, representing 210 scans per image. The 3D images displayed clear and bright spots (see Movie 2). Although SMCy7 and SMCy7.5 emit in the NIR region, where the sensitivity of the microscope's detectors is lower, they led to excellent 3D imaging due to the efficient excitation with the 635 nm laser (Figure S18).

Multicolor Imaging. Multicolor imaging provides important information and allows revealing different cellular processes on the same image. For this reason, it is of great importance to have available fluorescent markers with various excitation and emission wavelengths combined with narrow emission bands, thus allowing their concomitant use. A lambda scan experiment with the help of a laser scanning confocal microscope allowed us to obtain *in situ* emission spectra of Nile Red and the SMCy in the cell lipid droplets (Figure 7). It is noteworthy that unlike Nile Red, which was bright enough in the cytosplasm to provide a lambda scan emission spectrum (Figure 7D), SMCy dyes, due to their selective LD staining, did not provide any spectrum. The obtained spectra were similar to those obtained in oil using a fluorometer, confirming the localization of the dyes in a nonpolar lipophilic environment. In cell lipid droplets the SMCy displayed significantly narrower spectra than Nile Red (λ_{Em} max = 570 nm; fwhm = 86 nm).

For these reasons, we assumed that, unlike Nile Red, SMCy might be efficient in multicolor imaging. First, according to the obtained spectroscopic data in oil, we show that unlike Nile Red, SMCy3 can be used as a green LD marker and in combination with red-emitting fluorophores (Figure 8). Although both Nile Red and SMCy3 are efficiently excited with a 488 nm laser (70% and 62%, respectively), SMCy3 displays much narrower absorption and emission bands (fwhm: Abs 54 nm, Em: 49 nm), with a blue-shifted emission ($\lambda_{Em\ max}$

DOI: 10.1021/jacs.7b12817
J. Am. Chem. Soc. XXXX, XXX, XXX−XXX

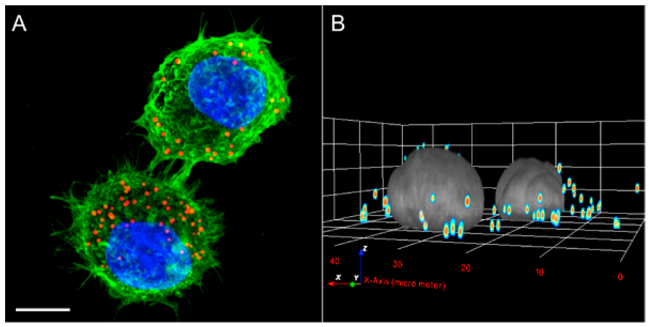

Figure 6. Images of KB cells incubated with SMCy5 (500 nM) then fixed (PFA 4%), obtained by a 21 μm depth Z-stack (300 nm stepwise) showing the repartition of the LDs within the cells. (A) Maximum intensity projection image displaying the LDs (red), the nucleus (blue), and the plasma membrane (green). (B) 3D image displaying the LDs (colored spots) and the nucleus (gray). The nucleus was stained with 5 μg/mL Hoechst; the plasma membrane, with MemBright-488 (200 nM). Incubation with SMCy5 was done in opti-MEM for 3 h. Scale bar is 10 μm.

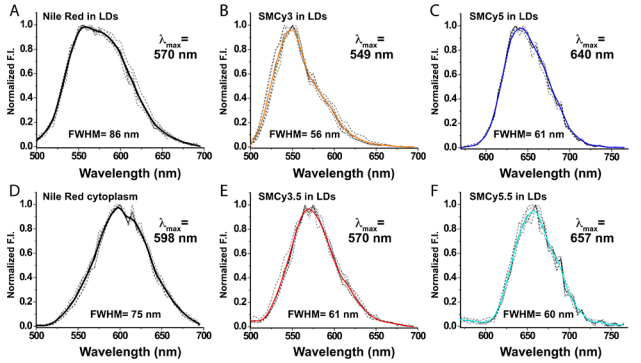

Figure 7. Normalized emission spectra of Nile Red in LDs (A) and in the cytoplasm (D) and normalized emission spectra of SMCy dyes in LDs obtained by lambda scan (5 nm steps) with a laser confocal microscope using the 488 nm laser (for Nile Red, SMCy3, and SMCy3.5) and the 560 nm laser (for SMCy5 and SMCy5.5). Dashed lines correspond to five independent measurements (normalized), which were averaged and smoothed (solid lines).

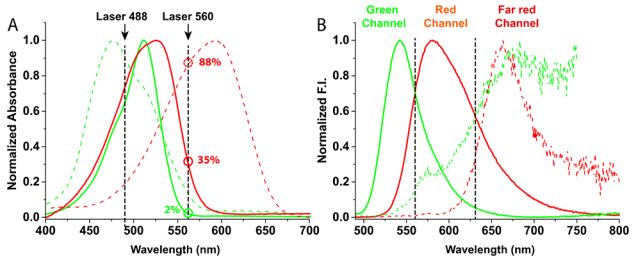

Figure 8. Normalized absorption (A) and emission (B) spectra of SMCy3 (green lines) and Nile Red (red lines) in colza oil (solid line) and in water (dashed lines). Concentration was 1 μM, and excitation was 480 nm.

541 nm), compared to Nile Red ($\lambda_{Em\ max}$ 581 nm, fwhm: Abs 80 nm, Em 84 nm). Moreover, Nile Red is also efficiently excited with the 560 nm laser (35% in oil), whereas SMCy3 is only excited at 2%. Finally, due to its solvatochromism, Nile Red when irradiated at 560 nm in water is efficiently excited (88%, Figure 8). Consequently, when Nile Red localizes in more polar cellular environments in the cytoplasm, its excitation and emission spectra shift to the red, thus leading to crosstalk in the red and far-red channels.

As a green-emitting LD probe was available (BODIPY 493/503),[23] we then wanted to show that SMCy3.5 could be used as a red LD marker in multicolor imaging. To this aim, KB cells were incubated with (1) Hoechst, a blue marker for the nucleus; (2) MitoTracker Green, a green marker for mitochondria,[23] and (3) Nile Red or SMCy3.5, as a red-emitting LD markers. Prior to the imaging, dSQ12S was used as a far-red plasma membrane marker.[55] The obtained multicolor imaging showed that whereas Nile Red displayed distinct crosstalk in the green channel (LDs) and in the far-red channel (cytoplasm), SMCy3.5, due to its sharp absorption and emission bands and its weak solvatochromism, displayed no crosstalk, thus leading to clear multicolor imaging (Figure 9). This set of experiments showed that, unlike Nile Red, SMCy3 and SMCy3.5 can be used as green and red lipid droplet markers, respectively, with no crosstalk in fluorescent microscopy imaging.

TISSUE IMAGING

Monophoton Imaging. Taking advantage of the brightness and specificity of the SMCy dyes, we investigated their ability to reveal lipid-rich structures/organelles in multicolor tissue imaging. For this purpose white adipose tissue of a mouse was incubated in the presence of Hoechst (nuclear staining), MemBright-488 (plasma membrane staining), and SMCy3.5. The tissue was then imaged by fluorescence microscopy (Figure 10). The obtained images allowed for 3D imaging (see Movie 3) as well as a projection that clearly shows that SMCy3.5 selectively stained the fat reservoirs of adipocytes (Figure 10B) but also revealed the presence of dots in the blood vessel that could be identified as low density lipoprotein (LDL) or circulatory LDs (Figure 10D).

TPE Imaging. Two-photon excitation microscopy imaging has received considerable attention as an advanced optical technique in the field of bioimaging for several reasons.[58−60] First, TPE microscopy inherently provides three-dimensional sectioning since the excitation occurs only at the focal point of the sample. In addition, due to its localized excitation with a NIR laser, it reduces the photobleaching, the phototoxicity, and the cell autofluorescence. It also ensures deeper tissue penetration, which enables experiments on thicker live samples. For these reasons, there is a high demand for bright fluorescent probes with high TPE cross-section values, leading to ongoing efforts to design such fluorophores.[61] To this aim, we first measured the TPA cross-section of SMCy dyes in a cuvette. The two-photon nature of the absorption process was verified from the quadratic dependence of the observed emission intensity vs excitation power (Figures S19 to S22).

The results showed that although SMCy7 and SMCy7.5 did not display TPE below 900 nm, the remaining dyes displayed higher TPA cross-section values (Figure 11) when compared to the known LDs probes.[29] While SMCy3 only possessed a modest TPA cross-section (178 GM at 690 nm), SMCy3.5 reaches values as high as 2400 GM (at 760 nm). Finally, SMCy5 and SMCy5.5 displayed impressive TPA cross-section values, 6250 GM at 740 nm and 13 330 GM at 770 nm, respectively.

Interestingly, SMCy5.5 displays a very high cross-section values of 10 400 GM at the commonly used 820 nm wavelength (used for rhodamine-based probes). Combined with its exceptional brightness in lipidic environments, this probe

DOI: 10.1021/jacs.7b12817
J. Am. Chem. Soc. XXXX, XXX, XXX−XXX

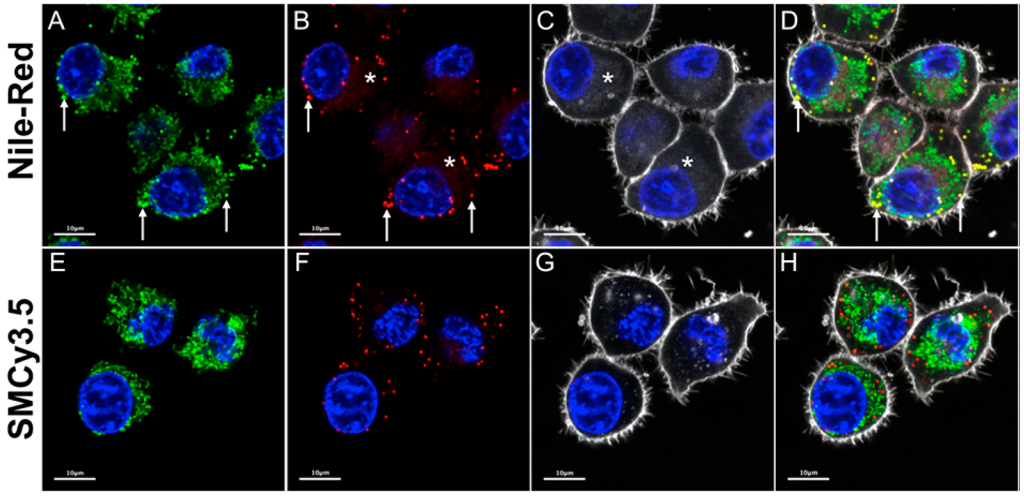

Figure 9. Laser scanning confocal microscopy images of live KB cells incubated 3 h with Hoechst (5 μg/mL, blue color), MitoTracker Green (200 nM), Nile Red, or SMCy3.5 (500 nM). Plasma membrane was stained prior to imaging with dSQ12S, a far-red-emitting plasma membrane probe (gray color). Green channel: A and E (ex: 488 nm, em: 498−540 nm); red channel: B and F (ex: 561 nm, em: 570−640 nm); far-red channel: C and G (ex: 632 nm, em: 640−750 nm). (D and H) Merging of A, B, C and E, F, G, respectively. White arrows and white stars indicate the crosstalk of Nile Red in the green and the far-red channels, respectively. Scale bar is 10 μm.

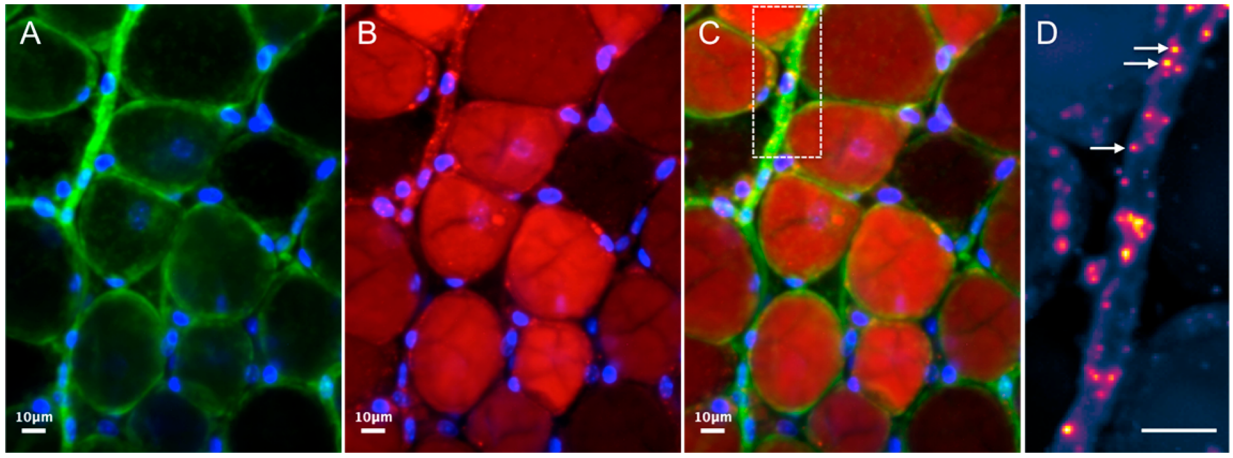

Figure 10. Images of adipocytes in mouse adipose tissue (25 μm depth) obtained by a maximum projection of a Z-stack (100 slices of 250 nm depth each). The tissue was incubated overnight at 4 °C with Hoechst (5 μg/mL, nuclei in blue color), (A) MemBright-488 (5 μM, plasma membrane in green color), and (B) SMCy3.5 (5 μM, lipid domains, red color). (C) Merged channels. (D) Zoomed-in region of interest in C showing the lipid-rich vesicles (white arrows) in the blood vessel. Scale bar is 10 μm.

constitutes one of the brightest two-photon-excitable fluorophores to date.

In light of the exceptional TPE brightness of SMCy, we mapped the lipophilic environment in tissue using multicolor TPE imaging. A mouse liver slice was incubated with Hoechst and SMCy5.5. Using only one excitation wavelength (810 nm), we obtained a 52 μm depth 3D image where the nuclei, the lipid droplets, and the collagen fibers (using second-harmonic generation[62,63]) were clearly distinguished (Figure 12). The image revealed large lipid-rich vesicles that are not present in the collagen-rich region.

Lipid Droplet Exchange. With multicolor LD markers in hand it becomes possible to monitor the fate of different LD populations in the same experiment. First, as a control experiment, a batch of KB cells was incubated with the same concentration of SMCy3.5 and SMCy5.5 for 3 h. The images showed a strong colocalization of the dyes within the same LDs, showing nondifferent uptake of the dyes (Figure 13A). It is noteworthy that although almost no green LDs were detected, some red LDs were observed. This might be attributed to the Forster resonance energy transfer (FRET) phenomenon occurring in some LDs and driven by the close proximity between the donor SMCy3.5 and the acceptor SMCy5.5. Second, two batches of KB cells were independently incubated with SMCy3.5 and SMCy5.5 for 3 h. After several washing steps to avoid cross contamination, the cells were trypsinized, mixed, plated, and cocultured. After 12 h, two distinct populations of cells could be identified by the color of their lipid droplets with no apparent exchange of LDs between cells showing no colocalization of the dyes (Figure 13B). This tends to prove that the dyes are confined in the LDs with no leakage out of the cells. After 48 h, the same sample of cells was visualized. Remarkably, within some cells, LDs of two distinct colors were observed (Figure 13C and D), suggesting LDs exchange between cells. In these cells the colocalization of the two dyes was also minimal, proving that the dyes were not exchanged within the LDs of the same cell. These experiments illustrate that KB cells are able to actively exchange LDs or that

DOI: 10.1021/jacs.7b12817
J. Am. Chem. Soc. XXXX, XXX, XXX−XXX

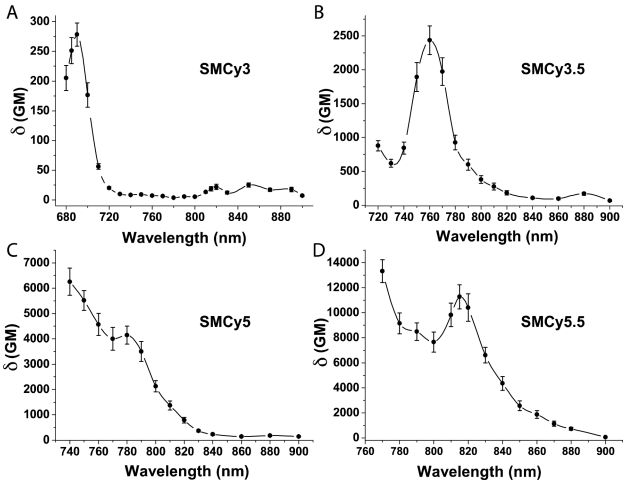

Figure 11. Two-photon-excitation cross-section spectra of SMCy dyes in DMSO. The reference used for measurements was rhodamine B. GM is Goeppert−Mayer unit.

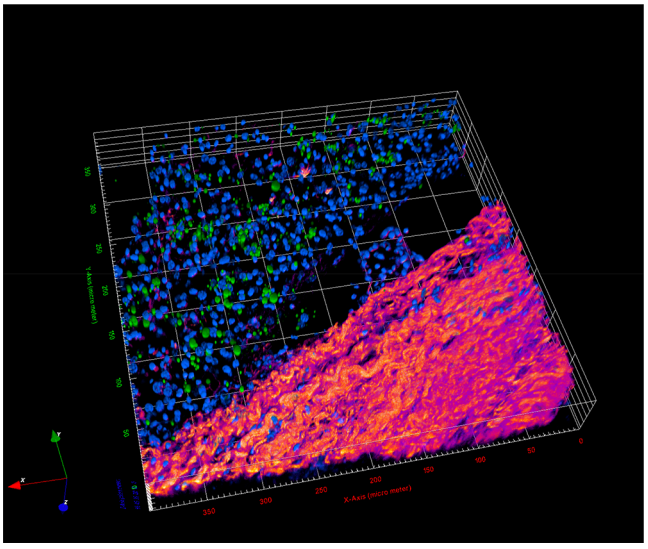

Figure 12. Two-photon excitation 3D imaging (52 μm depth) of a mouse liver slice, incubated with Hoechst (5 μg/mL) and SMCy5.5 (5 μM). The nuclei are displayed in blue, the lipid droplets in green, and the collagen fibers in fire color. The two-photon excitation wavelength was 810 nm.

cells are able to take up LDs released from dead cells. Owning to their photostability, brightness, and ability to remain in the LDs with no leakage, SMCy dyes constitute a robust tool to stain and track LDs in bioimaging experiments.

Functionalization of SMCy. SMCy dyes bear an alkyne side arm for further functionalization by CuAAC click chemistry. Indeed, owing to their interesting physicochemical properties (neutral fluorophores, high brightness, narrow absorption and emission bands), SMCy can serve as a platform to develop various selective markers or sensors. As an example, SMCy3 was involved in a click chemistry reaction with an azido triphenylphosphonium cation that is known to target mitochondria (Figure 14A).[64] The obtained SMCy3-M was then incubated for 1 h at 200 nM in the presence of KB cells. After checking that crosstalk did not occur (Figure S23), the colocalization experiment using MitoTracker Red led to a measured Pearson correlation coefficient of 0.96, thus proving

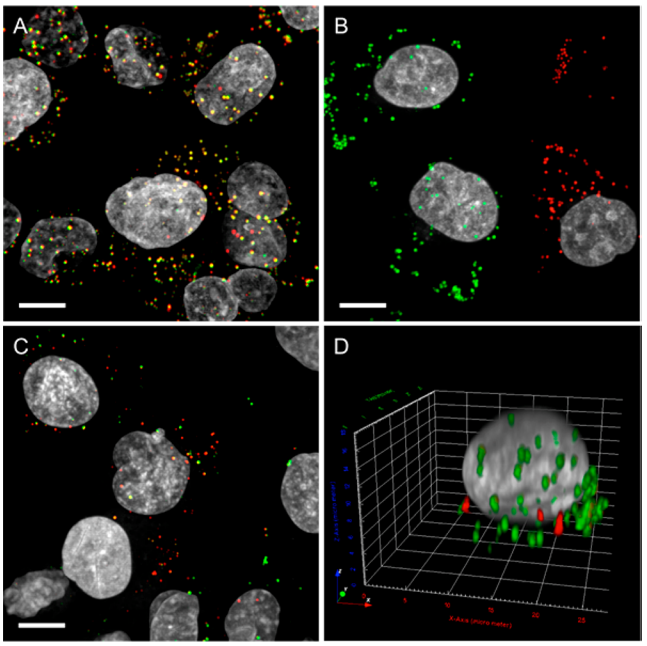

Figure 13. Images of live KB cells obtained by a maximum projection of a 20 μm depth Z-stack. (A) Co-incubation of SMCy3.5 (1 μM) and SMCy5.5 (1 μM) for 3 h then imaged after 18 h. (B) Coculture of KB cells incubated with SMCy3.5 and SMCy5.5 separately after 18 h. (C) Coculture of KB cells incubated with SMCy3.5 and SMCy5.5 separately after 48 h. (D) 3D view of a KB cell displaying LDs from another cell. Scale bar is 10 μm.

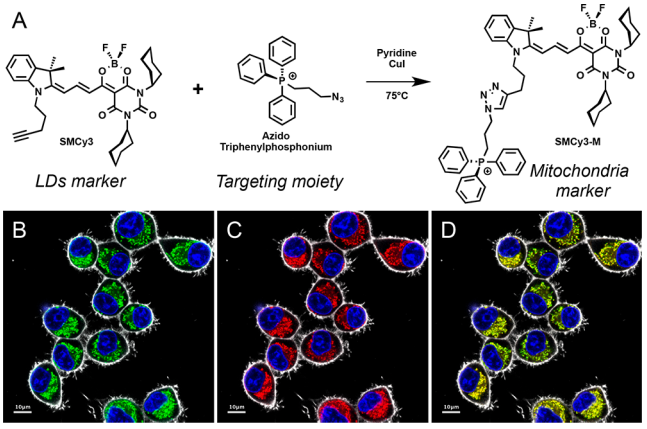

Figure 14. Synthesis of SMCy3-M by CuAAC click chemistry (A). Laser scanning confocal microscopy of live KB cells incubated for 1 h with Hoechst (5 μg/mg, blue color) and 200 nM of SMCy3-M (B) and MitoTracker Red CMXRos (C). (D) Merged images. The plasma membrane was stained with dSQ12S (20 nM) prior to imaging. Excitation wavelength and emission range for imaging in nm: Hoechst (405, 415−470), SMCy3-M (488, 498−560), MitoTracker Red (561, 571−620), and dSQ12S (635, 645−700). Scale bar is 10 μm.

that SMCy3 was successfully converted into an efficient and selective mitochondria marker (Figure 14).

CONCLUSION

In this work we designed and synthesized a new family of dioxaborine-containing merocyanines, named StatoMerocyanines. These fluorophores cover the visible spectrum and the NIR region with high brightness and photostability. SMCy were found to be soluble in both water and oil and exhibit an

DOI: 10.1021/jacs.7b12817
J. Am. Chem. Soc. XXXX, XXX, XXX−XXX

impressive fluorescence enhancement between these two environments. When incubated with cells, SMCy selectively stain the LDs in a bright and background-free manner, thus leading to high-quality images including multicolor 3D images. Owning to their sharp absorption and emission bands, SMCy were shown to be efficient for multicolor imaging (four colors) more particularly in the green and red channels, where Nile Red leads to crosstalk. SMCy served in multicolor tissue imaging, where it successfully probed the lipophilic environment in adipocytes as well as revealed circulating lipidic vesicles in the blood vessel. SMCy3 to SMCy5.5 are two-photon excitable, displaying impressive cross-section values up to 13 300 GM, making SMCy5.5 one of the brightest TPE fluorophores to date. These properties allowed obtaining multicolor TPE 3D-images revealing the distribution of lipidic vesicles in liver tissue. Benefiting from the different available colors of these LDs marker, we used them to track two populations of LDs and showed that LD exchange occurs between cells. Finally, we demonstrated that, using their alkyne group, SMCy can be derivatized by click chemistry in order to obtain fluorescent probes with different targeting specificity. This study should encourage the continuation in the development of new dioxaborine merocyanines for bioimaging.

MATERIALS AND METHODS

Synthesis. All starting materials for synthesis were purchased from Alfa Aesar, Sigma-Aldrich, or TCI Europe and used as received unless stated otherwise. NMR spectra were recorded on a Bruker Avance III 400 MHz spectrometer. Mass spectra were obtained using an Agilent Q-TOF 6520 mass spectrometer. Synthesis of all new compounds is described in the Supporting Information.

Spectroscopy. The water used for spectroscopy was Milli-Q water (Millipore), and all the solvents were spectral grade. Colza oil, mainly composed of unsaturated lipids ~93%, was obtained from Lesieur (Asnières-sur-Seine, France). Labrafac (Labrafac Lipophile WL 1349) is composed of medium-chain tiglycerides and caprylic/capric triglyceride and was obtained from Gattefossé (Saint Priest, France). Absorption and emission spectra were recorded on a Cary 400 Scan ultraviolet−visible spectrophotometer (Varian) and a FluoroMax-4 spectrofluorometer (Horiba Jobin Yvon) equipped with a thermostated cell compartment, respectively. For standard recording of fluorescence spectra, the emission was collected 10 nm after the excitation wavelength. All the spectra were corrected from the wavelength-dependent response of the detector. Quantum yields were determined by comparison with a reference according to their excitation and emission wavelengths: rhodamine 6G in water[65] was used as the reference for SMCy3 and SMCy3.5, DID in MeOH[66] for SMCy5 and SMCy5.5, and rhodamine 800 in EtOH[67] for SMCy7. For SMCy7.5, rhodamine 800 and indocyanine green in MeOH[68] were used depending on the solvent.

TPE Measurements. Two-photon-absorption cross-section measurements were performed using rhodamine B in methanol as a calibration standard according to the method of Webb et al.[69] Two-photon excitation was provided by an InSight DS+ laser (Spectra Physics) with a pulse duration of 120 fs. The laser was focused with an achromatic lens (f = 2 cm) in a cuvette containing the dye (SMCy3: 6.04 μM, SMCy3.5: 2.08 μM, SMCy5: 1.06 μM, SMCy5.5: 285 nM) in DMSO, and the spectra were recorded with a fibered spectrometer (Avantes) by collecting the fluorescence emission at 90° with a 20× Olympus objective.

X-ray Crystallography. Single crystals of SMCy7 were obtained by a solvent exchange method using DCM as solvent and cyclohexane as antisolvent.[70] X-ray diffraction data collection was carried out on a Bruker APEX II DUO Kappa-CCD diffractometer equipped with an Oxford Cryosystem liquid N_2 device, using Mo Kα radiation (λ = 0.710 73 Å). The crystal−detector distance was 38 mm. The cell parameters were determined (APEX2 software)[71] from reflections taken from three sets of 12 frames, each at 10 s exposure. The structure was solved by direct methods using the program SHELXS-2013.[72] The refinement and all further calculations were carried out using SHELXL-2013.[73] The H atoms were included in calculated positions and treated as riding atoms using SHELXL default parameters. The non-H atoms were refined anisotropically, using weighted full-matrix least-squares on F^2. A semiempirical absorption correction was applied using SADABS in APEX2;[71] transmission factors: T_{min}/T_{max} = 0.6697/0.7456.

Confocal Imaging. KB cells (ATCC CCL-17) were grown in minimum essential medium (MEM, Gibco-Invitrogen) with 10% fetal bovine serum (FBS, Lonza), 1% nonessential amino acids (Gibco-Invitrogen), 1% MEM vitamin solution (Gibco-Invitrogen), 1% L-glutamine (Sigma-Aldrich), and 0.1% antibiotic solution (gentamicin, Sigma-Aldrich) at 37 °C in a humidified atmosphere containing 5% CO_2. Cells were seeded onto a chambered coverglass (IBiDi) at a density of 5 × 10^4 cells/well 24 h before the microscopy measurement. For imaging, the culture medium was removed and the attached cells were washed with Opti-MEM (Gibco−Invitrogen). Next, the cells were incubated in Opti-MEM with Hoechst (5 μg/mL) to stain the nuclei and in the presence of Nile Red or SMCy dyes (0.5 to 1 μM) for 3 h. The living cells were washed three times with HBSS and visualized in HBSS or were fixed in 4% paraformaldehyde (PFA) in HBSS for 5 min before being washed three times in HBSS. The images were processed with Icy software.[74] The plasma membrane was stained with dSQ12S (200 nM) prior to imaging.[55] The Pearson's correlation coefficient was measure with the Colocalization Studio plugin[75] using Icy software.

Cytotoxicity Assay. The cytotoxicity assay of the SMCy dyes was quantified by the MTT assay (3-(4,5-dimethylthiazol-2-yl)-2,5-diphenyltetrazolium bromide). A total of 1 × 10^4 KB cells/well were seeded in a 96-well plate 24 h prior to the cytotoxicity assay in Dulbecco's modified Eagle's medium (Gibco Lifetechnologies, DMEM) complemented with 10% FBS, gentamicin (100 μg/mL), L-glutamine (2 mM), nonessential amino acids (1 mM), and MEM vitamin solution (1%) and were incubated in a 5% CO_2 incubator at 37 °C. After medium removal, 100 μL of DMEM containing 5, 1, or 0.2 μM SMCy (SMCy3, SMCy3.5, SMCy5, SMCy5.5, SMCy7, and SMCy7.5) was added to the KB cells and incubated for 3 h at 37 °C (5% CO_2). As a control, for each 96-well plate, the cells were incubated with DMEM containing the same percentage of DMSO (0.5% v/v) as the solution with the tested dyes or with Triton 1% as a positive control of cytotoxicity. After 3 h of dye incubation, the medium was replaced by 100 μL of a mix containing DMEM + MTT solution (diluted in phosphate-buffered saline (PBS) beforehand), and the cells were incubated for 4 h at 37 °C. Then, 75 μL of the mix was replaced by 50 μL of DMSO (100%) and gently shaken for 15 min at room temperature in order to dissolve the insoluble purple formazan reduced in living cells. The absorbance at 540 nm was measured (absorbances of the dyes at 540 nm were taken into account). Each concentration of dye was tested in sextuplicate in three independent assays. For each concentration, we calculated the percentage of cell viability in reference to the control DMEM + 0.5% DMSO.

Tissue Imaging. C57BL6/J mice were maintained on a 12 h light−dark cycle with *ad libitum* access to food and water. All animal work was conducted following a protocol approved by the ethical committee. Adult C57BL6 mice were euthanized by CO_2 administration. Liver and fat pads were immediately dissected and washed in PBS at 4 °C. The liver was sliced into 1 mm slices on a Leica vibratome. Tissues were placed overnight at 4 °C in 1 mL of freshly prepared solution of dye. Adipose tissue: SMCy3.5: 5 μM, MemBright-488, 5 μM, and Hoechst: 5 μg/mL in PBS. Liver tissue: SMCy5.5: 5 μM and Hoechst: 5 μg/mL in PBS. The tissue samples were washed three times with PBS before being placed in a homemade glass chamber, allowing the imaging on both sides of the slides. Briefly a 1 cm diameter hole was breached in the glass slide using a diamond drill bit. The 1 mm tissue slice was inserted in the hole, covered by a coverslip (170 nm, #1.5) on each slide, and sealed with Picodent Twinsil. The adipose tissue slices were imaged with a Leica DMi8 microscope equipped with a spinning disc CSU-X1. The microscopy

DOI: 10.1021/jacs.7b12817
J. Am. Chem. Soc. XXXX, XXX, XXX−XXX

settings were as follows: Hoechst (ex 405 nm, em 450 ± 60), MemBright-488 (ex 488 nm, em 510 ± 23), SMCy3.5 (ex 561 nm, em 590 ± 35). The images were acquired with a 0.37 pixel width in XY and 0.5 μm in Z with a PL APO 20×/0.75 oil immersion Leica objective. The images were processed with Icy software. For two-photon imaging see below.

Two-Photon Imaging. Two-photon fluorescence microscopy imaging was performed on a TriMScope II (LaVision BioTec, Bielefeld, Germany) built on an Olympus BX51 microscope. The excitation source was a tunable InSight laser (Spectra Physics) (range 690−1300 nm, repetition rate 80 MHz). For our experiments the excitation wavelength was fixed at 810 nm. Each line was scanned twice (line average 2) with a speed of 0.4 μs per pixel using a 20× Plan Apo NA:1 water immersion objective, with a working distance of 2 mm (Carl Zeiss, Germany). A Z-stack of 66 images was aquired with a Z-step of 0.8 μm for a total depth of 52 μm. The fluorescence signal was detected backward with sensitive gallium arsenide phosphide detectors (GaAsp). We used bandpass filters for the detection, more precisely for the collagen fiber and the SHG signal at 400−410 nm, the Hoechst at 435−485 nm, and the SMCy5.5 at 655−685 nm. The images were processed with Icy software.

Lipid Droplet Exchange Experiments. KB cells were seeded on T-25 flasks at a density of 1.5×10^6 cells before the day of the LD staining. The next day the medium was removed and the adhered cells were rinsed with PBS two times. Then, the cells were separately incubated with SMCy3.5 or SMCy5.5 (1 μM in OptiMEM 0.5% DMSO) at 37 °C, 90% humidity, 5% CO_2 for 3 h. After incubation the media containing the dyes were discharged, and KB cells were rinsed with PBS two times, growth medium to ensure a proper removal of the excess dyes, and PBS again. Cells were trypsinised and centrifuged at 15 000 rpm for 3 min, and the pellets of cells were resuspended in growth medium. The suspensions of cells were centrifuged again, and cells were resuspended in the growth medium. Both fractions of cells were thoroughly mixed together in the same amount (~6×10^6 in total). The cells were seeded onto a chambered coverglass (IBiDi) at a density of 1×10^5 cells/well. Prior to imaging, cells were incubated with Hoechst (5 μg/mL) for 15 min for nucleus staining. The cells were then fixed with PFA 4% for 5 min and washed three times with HBSS. Images were taken after 18 and 48 h post cell adherence with spinning-disk microscopy. For this purpose, a Nikon Ti-E inverted microscope, equipped with CFI Plan Apo 60× oil (NA = 1.4) objective, an X-Light spinning disk module (CresOptics), and a Hamamatsu Orca Flash 4 sCMOS camera, was used. The microscopy settings were as follows: Hoechst (ex 405 nm, em 510 ± 42 nm), SMCy3.5 (ex 532 nm, em 600 ± 25 nm), SMCy5.5 (ex 638 nm, em 705 ± 36 nm). The images were recorded using NIS Elements and then processed with Icy software.

■ ASSOCIATED CONTENT

Supporting Information

The Supporting Information is available free of charge on the ACS Publications website at DOI: 10.1021/jacs.7b12817.

Synthesis, protocols, characterizations, and spectra (PDF)

Movies (ZIP)

X-ray crystallographic data (CIF)

■ AUTHOR INFORMATION

Corresponding Author

*mayeul.collot@unistra.fr

ORCID

Mayeul Collot: 0000-0002-8673-1730

Andrey S. Klymchenko: 0000-0002-2423-830X

Notes

The authors declare no competing financial interest.

■ ACKNOWLEDGMENTS

We thank Romain Vauchelles for his assistance at the PIQ imaging platform and Bogdan Andreiuk for providing us with compound **1**. We thank the national research group GDR Imabio for promoting interdisplinary meetings. We acknowledge the Service de Chimie Analytique (SCA) for LC-MS and RMN analyses. We also acknowledge the ImagoSeine core facility of the Institut Jacques Monod, members of IBiSA and the France-BioImaging infrastructure, and supported by ANR grant (ANR-10-INBS-04). This work was supported by ERC Consolidator grant BrightSens 648528, and ANR BrightRiboProbes (ANR-16-CE11-0010) and ANR grant (ANR-10-INBS-04).

■ REFERENCES

(1) Farese, R. V.; Walther, T. C. *Cell* **2009**, *139*, 855−860.
(2) Martin, S.; Parton, R. G. *Nat. Rev. Mol. Cell Biol.* **2006**, *7*, 373−378.
(3) Walther, T. C.; Farese, R. V., Jr *Annu. Rev. Biochem.* **2012**, *81*, 687−714.
(4) Thiam, A. R.; Farese, R. V., Jr.; Walther, T. C. *Nat. Rev. Mol. Cell Biol.* **2013**, *14*, 775−786.
(5) Zehmer, J. K.; Huang, Y.; Peng, G.; Pu, J.; Anderson, R. G. W.; Liu, P. *Proteomics* **2009**, *9*, 914−921.
(6) Blom, T.; Somerharju, P.; Ikonen, E. *Cold Spring Harbor Perspect. Biol.* **2011**, *3*, a00471310.1101/cshperspect.a004713.
(7) Olzmann, J. A.; Richter, C. M.; Kopito, R. R. *Proc. Natl. Acad. Sci. U. S. A.* **2013**, *110*, 1345−1350.
(8) Bozza, P. T.; Viola, J. P. B. *Prostaglandins, Leukotrienes Essent. Fatty Acids* **2010**, *82*, 243−250.
(9) Krahmer, N.; Farese, R. V.; Walther, T. C. *EMBO Mol. Med.* **2013**, *5*, 973−983.
(10) Herker, E.; Harris, C.; Hernandez, C.; Carpentier, A.; Kaehlcke, K.; Rosenberg, A. R.; Farese, R. V.; Ott, M. *Nat. Med.* **2010**, *16*, 1295−1298.
(11) Tirinato, L.; Pagliari, F.; Limongi, T.; Marini, M.; Falqui, A.; Seco, J.; Candeloro, P.; Liberale, C.; Di Fabrizio, E. *Stem Cells Int.* **2017**, *2017*, 1.
(12) Liu, Q.; Luo, Q.; Halim, A.; Song, G. *Cancer Lett.* **2017**, *401*, 39−45.
(13) Abramczyk, H.; Surmacki, J.; Kopeć, M.; Olejnik, A. K.; Lubecka-Pietruszewska, K.; Fabianowska-Majewska, K. *Analyst* **2015**, *140*, 2224−2235.
(14) Lavis, L. D. *Annu. Rev. Biochem.* **2017**, *86*, 825−843.
(15) Zhu, H.; Fan, J.; Du, J.; Peng, X. *Acc. Chem. Res.* **2016**, *49*, 2115−2126.
(16) Yang, Y.; Zhao, Q.; Feng, W.; Li, F. *Chem. Rev.* **2013**, *113*, 192−270.
(17) Kobayashi, H.; Ogawa, M.; Alford, R.; Choyke, P. L.; Urano, Y. *Chem. Rev.* **2010**, *110*, 2620−2640.
(18) Nadler, A.; Schultz, C. *Angew. Chem., Int. Ed.* **2013**, *52*, 2408−2410.
(19) Li, X.; Gao, X.; Shi, W.; Ma, H. *Chem. Rev.* **2014**, *114*, 590−659.
(20) Su, D.; Teoh, C. L.; Wang, L.; Liu, X.; Chang, Y.-T. *Chem. Soc. Rev.* **2017**, *46*, 4833−4844.
(21) Klymchenko, A. S. *Acc. Chem. Res.* **2017**, *50*, 366−375.
(22) Greenspan, P.; Mayer, E. P.; Fowler, S. D. *J. Cell Biol.* **1985**, *100*, 965−973.
(23) Life Technologies https://www.thermofisher.com/.
(24) Spandl, J.; White, D. J.; Peychl, J.; Thiele, C. *Traffic* **2009**, *10*, 1579−1584.
(25) Wang, Z.; Gui, C.; Zhao, E.; Wang, J.; Li, X.; Qin, A.; Zhao, Z.; Yu, Z.; Tang, B. Z. *ACS Appl. Mater. Interfaces* **2016**, *8*, 10193−10200.
(26) Sharma, A.; Umar, S.; Kar, P.; Singh, K.; Sachdev, M.; Goel, A. *Analyst* **2015**, *141*, 137−143.
(27) Appelqvist, H.; Stranius, K.; Börjesson, K.; Nilsson, K. P. R.; Dyrager, C. *Bioconjugate Chem.* **2017**, *28*, 1363−1370.

DOI: 10.1021/jacs.7b12817
J. Am. Chem. Soc. XXXX, XXX, XXX−XXX

(28) Kang, M.; Gu, X.; Kwok, R. T. K.; Leung, C. W. T.; Lam, J. W. Y.; Li, F.; Tang, B. Z. *Chem. Commun.* **2016**, *52*, 5957−5960.
(29) Jiang, M.; Gu, X.; Lam, J. W. Y.; Zhang, Y.; Kwok, R. T. K.; Wong, K. S.; Tang, B. Z. *Chem. Sci.* **2017**, *8*, 5440−5446.
(30) Gonçalves, M. S. T. *Chem. Rev.* **2009**, *109*, 190−212.
(31) Sun, W.; Guo, S.; Hu, C.; Fan, J.; Peng, X. *Chem. Rev.* **2016**, *116*, 7768−7817.
(32) Chan, J.; Dodani, S. C.; Chang, C. J. *Nat. Chem.* **2012**, *4*, 973−984.
(33) Kamada, K.; Namikawa, T.; Senatore, S.; Matthews, C.; Lenne, P.-F.; Maury, O.; Andraud, C.; Ponce-Vargas, M.; Le Guennic, B.; Jacquemin, D.; Agbo, P.; An, D. D.; Gauny, S. S.; Liu, X.; Abergel, R. J.; Fages, F.; D'Aléo, A. *Chem. - Eur. J.* **2016**, *22*, 5219−5232.
(34) Kim, E.; Felouat, A.; Zaborova, E.; Ribierre, J.-C.; Wu, J. W.; Senatore, S.; Matthews, C.; Lenne, P.-F.; Baffert, C.; Karapetyan, A.; Giorgi, M.; Jacquemin, D.; Ponce-Vargas, M.; Guennic, B. L.; Fages, F.; D'Aléo, A. *Org. Biomol. Chem.* **2016**, *14*, 1311−1324.
(35) Zhou, Y.; Chen, Y.-Z.; Cao, J.-H.; Yang, Q.-Z.; Wu, L.-Z.; Tung, C.-H.; Wu, D.-Y. *Dyes Pigm.* **2015**, *112*, 162−169.
(36) Pfister, A.; Zhang, G.; Zareno, J.; Horwitz, A. F.; Fraser, C. L. *ACS Nano* **2008**, *2*, 1252−1258.
(37) Contreras, J.; Xie, J.; Chen, Y. J.; Pei, H.; Zhang, G.; Fraser, C. L.; Hamm-Alvarez, S. F. *ACS Nano* **2010**, *4*, 2735−2747.
(38) Kerr, C.; DeRosa, C. A.; Daly, M. L.; Zhang, H.; Palmer, G. M.; Fraser, C. L. *Biomacromolecules* **2017**, *18*, 551−561.
(39) Pitter, D. R.; Brown, A.; Baker, J.; Wilson, J. *Org. Biomol. Chem.* **2015**, *13*, 9477−9484.
(40) DeRosa, C. A.; Samonina-Kosicka, J.; Fan, Z.; Hendargo, H. C.; Weitzel, D. H.; Palmer, G. M.; Fraser, C. L. *Macromolecules* **2015**, *48*, 2967−2977.
(41) DeRosa, C. A.; Seaman, S. A.; Mathew, A. S.; Gorick, C. M.; Fan, Z.; Demas, J. N.; Peirce, S. M.; Fraser, C. L. *ACS Sens.* **2016**, *1*, 1366−1373.
(42) Wilson, J. N.; Wigenius, J.; Pitter, D. R. G.; Qiu, Y.; Abrahamsson, M.; Westerlund, F. *J. Phys. Chem. B* **2013**, *117*, 12000−12006.
(43) Pitter, D. R. G.; Wigenius, J.; Brown, A. S.; Baker, J. D.; Westerlund, F.; Wilson, J. N. *Org. Lett.* **2013**, *15*, 1330−1333.
(44) Karpenko, I. A.; Niko, Y.; Yakubovskyi, V. P.; Gerasov, A. O.; Bonnet, D.; Kovtun, Y. P.; Klymchenko, A. S. *J. Mater. Chem. C* **2016**, *4*, 3002−3009.
(45) Easton, T. G.; Valinsky, J. E.; Reich, E. *Cell* **1978**, *13*, 475−486.
(46) Zyabrev, K.; Doroshenko, A.; Mikitenko, E.; Slominskii, Y.; Tolmachev, A. *Eur. J. Org. Chem.* **2008**, *2008*, 1550−1558.
(47) Gerasov, A. O.; Shandura, M. P.; Kovtun, Y. P. *Dyes Pigm.* **2008**, *77*, 598−607.
(48) Gerasov, A. O.; Shandura, M. P.; Kovtun, Y. P. *Dyes Pigm.* **2008**, *79*, 252−258.
(49) Gerasov, A. O.; Zyabrev, K. V.; Shandura, M. P.; Kovtun, Y. P. *Dyes Pigm.* **2011**, *89*, 76−85.
(50) Gieseking, R. L.; Mukhopadhyay, S.; Risko, C.; Marder, S. R.; Brédas, J.-L. *Chem. Mater.* **2014**, *26*, 6439−6447.
(51) Frischmann, P. D.; Würthner, F. *Org. Lett.* **2013**, *15*, 4674−4677.
(52) Ozdemir, T.; Atilgan, S.; Kutuk, I.; Yildirim, L. T.; Tulek, A.; Bayindir, M.; Akkaya, E. U. *Org. Lett.* **2009**, *11*, 2105−2107.
(53) Ernst, L. A.; Gupta, R. K.; Mujumdar, R. B.; Waggoner, A. S. *Cytometry* **1989**, *10*, 3−10.
(54) Padilha, L.; Webster, S.; Przhonska, O.; Hu, H.; Peceli, D.; Rosch, J.; Bondar, M.; Gerasov, A.; Kovtun, Y.; Shandura, M.; Kachkovski, A.; Hagan, D.; Stryland, E. W. V. *J. Mater. Chem.* **2009**, *19*, 7503−7513.
(55) Collot, M.; Kreder, R.; Tatarets, A. L.; Patsenker, L. D.; Mely, Y.; Klymchenko, A. S. *Chem. Commun.* **2015**, *51*, 17136−17139.
(56) Lavis, L. D. *Biochemistry* **2017**, *56*, 5165−5170.
(57) Lavis, L. D.; Raines, R. T. *ACS Chem. Biol.* **2014**, *9*, 855−866.
(58) Helmchen, F.; Denk, W. *Nat. Methods* **2005**, *2*, 932−940.
(59) Svoboda, K.; Yasuda, R. *Neuron* **2006**, *50*, 823−839.
(60) Piston, D. W. *Trends Cell Biol.* **1999**, *9*, 66−69.
(61) Yao, S.; Belfield, K. D. *Eur. J. Org. Chem.* **2012**, *2012*, 3199−3217.
(62) Mohler, W.; Millard, A. C.; Campagnola, P. J. *Methods* **2003**, *29*, 97−109.
(63) Chen, X.; Nadiarynkh, O.; Plotnikov, S.; Campagnola, P. J. *Nat. Protoc.* **2012**, *7*, 654−669.
(64) Smith, R. A. J.; Porteous, C. M.; Gane, A. M.; Murphy, M. P. *Proc. Natl. Acad. Sci. U. S. A.* **2003**, *100*, 5407−5412.
(65) Magde, D.; Rojas, G. E.; Seybold, P. G. *Photochem. Photobiol.* **1999**, *70*, 737−744.
(66) Texier, I.; Goutayer, M.; Da Silva, A.; Guyon, L.; Djaker, N.; Josserand, V.; Neumann, E.; Bibette, J.; Vinet, F. *J. Biomed. Opt.* **2009**, *14*, 054005−11.
(67) Alessi, A.; Salvalaggio, M.; Ruzzon, G. *J. Lumin.* **2013**, *134*, 385−389.
(68) Benson, R.; Kues, H. *Phys. Med. Biol.* **1978**, *23*, 159−163.
(69) Albota, M. A.; Xu, C.; Webb, W. W. *Appl. Opt.* **1998**, *37*, 7352−7356.
(70) Spingler, B.; Schnidrig, S.; Todorova, T.; Wild, F. *CrystEngComm* **2012**, *14*, 751−757.
(71) *M86-E01078 APEX2 User Manual*; Bruker AXS Inc.: Madison, WI, USA, 2006.
(72) Sheldrick, G. M. *Acta Crystallogr., Sect. A: Found. Crystallogr.* **1990**, *46*, 467−473.
(73) Sheldrick, G. M. *Acta Crystallogr., Sect. A: Found. Crystallogr.* **2008**, *64*, 112−122.
(74) Chaumont, F. de; Dallongeville, S.; Chenouard, N.; Hervé, N.; Pop, S.; Provoost, T.; Meas-Yedid, V.; Pankajakshan, P.; Lecomte, T.; Montagner, Y. L.; Lagache, T.; Dufour, A.; Olivo-Marin, J.-C. *Nat. Methods* **2012**, *9*, 690.
(75) Lagache, T.; Sauvonnet, N.; Danglot, L.; Olivo-Marin, J.-C. *Cytometry, Part A* **2015**, *87*, 568−579.

DOI: 10.1021/jacs.7b12817
J. Am. Chem. Soc. XXXX, XXX, XXX−XXX